Available online at www.sciencedirect.com
ScienceDirect
Biochimica et Biophysica Acta 1778 (2008) 1181–1189
Biochimica et Biophysica Acta
BBA
www.elsevier.com/locate/bbamem

Formation of aquaporin-4 arrays is inhibited by palmitoylation of N-terminal cysteine residues

Hiroshi Suzuki [a], Kouki Nishikawa [a], Yoko Hiroaki [a,b], Yoshinori Fujiyoshi [a,b,*]

[a] *Department of Biophysics, Faculty of Science, Kyoto University, Kitashirakawa-oiwake, Sakyo, Kyoto 606-8502, Japan*
[b] *Core Research for Evolution Science and Technology, Japan Science and Technology Agency, Kyoto, Japan*

Received 23 October 2007; received in revised form 9 December 2007; accepted 11 December 2007
Available online 15 December 2007

Abstract

Tetramers of the mammalian water channel aquaporin-4 (AQP4) assemble into square arrays and mediate bidirectional water transport across the blood–brain interface. The *aqp4* gene expresses two splicing isoforms. Only the shorter AQP4M23 isoform assembles into square arrays, while the longer AQP4M1 isoform interferes with array formation, presumably due to the additional 22 N-terminal residues. To understand why the N-terminus of AQP4M1 interferes with array formation, we constructed a series of N-terminal deletion mutants and examined their ability to form square arrays in Chinese hamster ovary (CHO) cells using SDS-digested freeze fracture replica labeling. Mutants with deletions of less than seventeen N-terminal residues did not form square arrays and showed dispersed immunogold labels against AQP4 molecules, whereas more deletions led to the formation of square arrays labeled with immunogolds. Furthermore, mutagenic substitution of the two cysteine residues at the position 13 and 17 in the N-terminus of AQP4M1 also resulted in the square array formation. Biochemical analysis and metabolic labeling of transfected CHO cells revealed that the two N-terminal cysteines of AQP4M1 are palmitoylated. These results suggest that palmitoylation of the N-terminal cysteines is the reason for the inability of AQP4M1 to form square arrays.

Keywords: Water channel; Square array; Palmitoylation; Freeze fracture; SDS-FRL; Electron microscopy

1. Introduction

Water channels of the aquaporin (AQP) family are found from archaea to animals and plants [1]. Thirteen water channels have been identified in humans, which fall into two classes: aquaporins, the pure water channels, and aquaglyceroporins, which in addition to water also permeate small, uncharged solutes. The first structure of an AQP, human AQP1, was analyzed by electron crystallography [2]. It revealed that each subunit in the AQP1 tetramer contains six transmembrane helices and two short helices forming a water selective pore. Although the permeability characteristics and structures are known for some of the mammalian AQPs [3], other information is still lacking. For example, while it has been established that the trafficking of AQP2 from intracellular vesicles to the apical membrane in the renal collecting duct is regulated by phosphorylation [4], little is known about how the function, expression and distribution of the other human AQPs are regulated.

AQP4 is a specific water channel that is predominantly expressed in the brain. More specifically, AQP4 is expressed in ependymal cells and retinal Müller cells as well as in astrocytes, in which AQP4 is localized to plasma membrane regions of glial end-feet that face blood vessels and the pia [5]. The specific localization of AQP4 appears to contribute to facilitate the bidirectional water flow across blood–brain interfaces [6–8]. Early freeze fracture electron microscopy studies revealed prominent arrays of orthogonally arranged intramembrane particles (IMPs) in the perivascular membranes of astrocyte end-feet [9]. Such square arrays have also been found in the basolateral membranes of renal collecting ducts [10] and the sarcolemmas of

Abbreviations: AQP, aquaporin; CHO, Chinese hamster ovary; IMP, intramembrane particle; SDS-FRL, SDS-digested freeze fracture replica labeling; P-face, protoplasmic fracture face; E-face, exoplasmic fracture face; ABE, acyl-biotinyl exchange; NEM, *N*-ethylmaleimide; AP, Alkaline Phosphatase

* Corresponding author. Department of Biophysics, Faculty of Science, Kyoto University, Kitashirakawa-oiwake, Sakyo, Kyoto 606-8502, Japan. Tel.: +81 075 753 4215; fax: +81 075 743 4218.
E-mail address: yoshi@em.biophys.kyoto-u.ac.jp (Y. Fujiyoshi).

0005-2736/$ - see front matter © 2007 Elsevier B.V. All rights reserved.
doi:10.1016/j.bbamem.2007.12.007

myofibers [11], both tissues that also express AQP4. Later studies using immunogold labeling of freeze fracture replicas provided direct evidence that AQP4 is the major constituent of the square arrays [12]. While the function of these arrays in the brain remains unclear, square arrays were reported to rapidly shrink or even disappear after circulatory arrest [13], indicating that the assembly of AQP4 tetramers into square arrays changes in response to the physiological conditions of the water homeostasis in the brain.

AQP4 has two alternative splice variants resulting from differential translation initiation either at the first methionine (AQP4M1, 323 aa) or at the second methionine (AQP4M23, 301 aa) [14]. As a result, AQP4M1 has a 22 residues longer N-terminus than AQP4M23. Endogenous AQP4 is considered to form heterotetramers containing both isoforms *in vivo*, but SDS-PAGE analysis showed that in rat brain and other tissues AQP4M23 is much more abundant than AQP4M1 [15]. While the water permeabilities of AQP4M1 and AQP4M23 are likely to be similar [14,15], freeze fracture analyses of CHO cells expressing AQP4M1 or AQP4M23 revealed that the two isoforms have different morphological properties. AQP4M23 can form large square arrays, whereas AQP4M1 restricts the formation of square arrays [16,17]. Co-expression of AQP4M1 and AQP4M23 leads to square arrays that are similar in size to those seen in astrocytes, implying that regulation mechanisms exist that may define the size and disassembly efficiency of square arrays.

The structure of rat AQP4M23 was determined by electron crystallography of two-dimensional (2D) crystals [18]. The packing of the tetramers in the 2D crystals, which resembled the one seen in *in vivo* square arrays, was stabilized by intermolecular interactions between amino acid residues of the transmembrane domains. This packing of AQP4 contrasted with that of the AQP0 arrays, which were stabilized by lipid–protein interactions [19–22]. The characteristic intermolecular interactions in AQP4 crystals were mediated by Arg108 and Tyr250, while further hydrophobic interactions were mediated by Gly157, Trp231, and Ile239, which are conserved in other AQPs. We proposed a mechanism regulating array disassembly based on competition experiments using peptides with Wild Type (WT) and mutated sequences of the AQP4M1 N-terminus. Our results suggested that Arg9, which is conserved in AQP4 proteins from different species, was the key residue in the destabilization of square arrays [18]. Since this idea was solely based on the structure of AQP4 in 2D crystals, it was necessary to test this hypothesis in living cells.

To elucidate the structural mechanism that regulates array formation, we constructed systematic N-terminal deletion mutants of AQP4 and examined their abilities to form square arrays by using SDS-digested freeze fracture replica labeling (SDS-FRL) [23] to directly visualize the distribution of AQP4 molecules in transiently transfected CHO cells. We identified two cysteine residues, only present in the longer N-terminus of AQP4M1, that are essential in disrupting the formation of square arrays. Further biochemical studies revealed that the N-terminal cysteines are post-translationally modified with palmitic acid. We thus propose palmitoylation as a new mechanism regulating the formation of AQP4 square arrays.

2. Materials and methods

2.1. Chemicals and antibody

Paraformaldehyde was purchased from TAAB (Berkshire, UK), polyvinyl formal (Formvar) from Okenshoji (Tokyo, Japan), [^{3}H]-palmitic acid (1.147 TBq/mmol) from PerkinElmer (Boston, MA, USA), and antibody against the C-terminus of AQP4 (anti-AQP4CT: rabbit polyclonal IgG, SC-20812) from Santa Cruz Biotechnology (Santa Cruz, CA, USA).

2.2. Construction of expression vectors

cDNAs for WT rat AQP4M1 and AQP4M23 were cloned from a rat brain cDNA library by PCR amplification. N-terminal deletion mutants were constructed by PCR from WT rat AQP4M1 cDNA and then subcloned into the pGEM-T Easy Vector (Promega). Cysteine substitutions were introduced using the QuickChange II Site-Directed Mutagenesis Kit (Stratagene). A 5′-KOZAK sequence (GCCACC) was added to each AQP4 construct just before the start codon. All constructs were confirmed by DNA sequencing. For expression, AQP4 constructs were cloned into the pcDNA3.1 (+) Vector (Invitrogen).

2.3. Expression

CHO-K1 cells were cultured in Dulbecco's modified Eagle's medium (DMEM) (SIGMA) containing 10% fetal bovine serum (BioWhittaker) and antibiotics. Cells were transfected with expression vectors using Lipofectamine 2000 according to the manufacturer's protocol (Invitrogen) with a slight modification to lower the toxicity. Opti-MEM I (Invitrogen) was used as culture medium during transfection and was replaced with serum-supplemented DMEM 2 h after transfection. For immunoblotting, transfected cells were harvested 24 h after transfection, lysed with 1% 3-[(3-cholamidopropyl) dimethylammonio]-1-propanesulfonate (CHAPS) (Dojindo, Kumamoto, Japan) in phosphate-buffered saline (PBS: 9.7 mM sodium phosphate, 1.5 mM potassium phosphate, 137 mM NaCl, 2.7 mM KCl, pH 7.4), and subjected to Western blot analysis with anti-AQP4CT antibody. Cell lines stably expressing AQP4 constructs were selected using 800 μg/ml Geneticin (Invitrogen) for 2 weeks after transfection.

2.4. SDS-FRL

SDS-FRL was performed as described previously [23,24] with the following modifications. Cells transiently expressing AQP4 constructs were scraped 24 h after transfection and cells stably expressing AQP4 constructs just before confluence. The cells were pelleted in phosphate buffer (PB: 100 mM sodium phosphate, pH 7.2), and fixed overnight at 37 °C with 4% formaldehyde (freshly depolymerized from paraformaldehyde) in PB. Fixed cells were washed with PB and cryo-protected by incubation in 30% glycerol in PB for 16 h at 4 °C. Cell suspensions mounted on flat specimen carriers (ϕ 3 mm; Bal-Tec, Balzers, Liechtenstein) were frozen by immersion in liquid nitrogen and fractured with a cooled metal knife in a freeze-etching system (BAF060; Bal-Tec) at −120 °C. The fractured faces were unidirectionally shadowed with platinum/carbon (2 nm) at an angle of 60°, followed by rotational carbon evaporation (20 nm) from the top. The pieces of replica were transferred to SDS digestion buffer (2.5% SDS in 15 mM Tris–HCl, pH 8.3, 20% sucrose) and incubated for 20 min at 121 °C in an autoclave. After cooling to room temperature, the replicas were washed three times with washing buffer (25 mM Tris–HCl, pH 7.4, 137 mM NaCl, 2.7 mM KCl, 0.1% Tween-20, 0.05% BSA, 0.05% NaN_3), blocked for 30 min in blocking buffer (5% BSA in washing buffer), and incubated with anti-AQP4CT antibody (0.4 μg/ml in blocking buffer) for 16 h at 4 °C. The replicas were washed again three times with washing buffer, blocked for 30 min in blocking buffer, and incubated with goat anti-rabbit IgG secondary antibodies coupled to 15 nm gold particles (BBInternational, Cardiff, UK) (1:50 dilution in blocking buffer) for 1 h at room temperature. The replicas were washed three times with washing buffer, twice with distilled water, and mounted on 100-mesh grids pre-coated with Formvar.

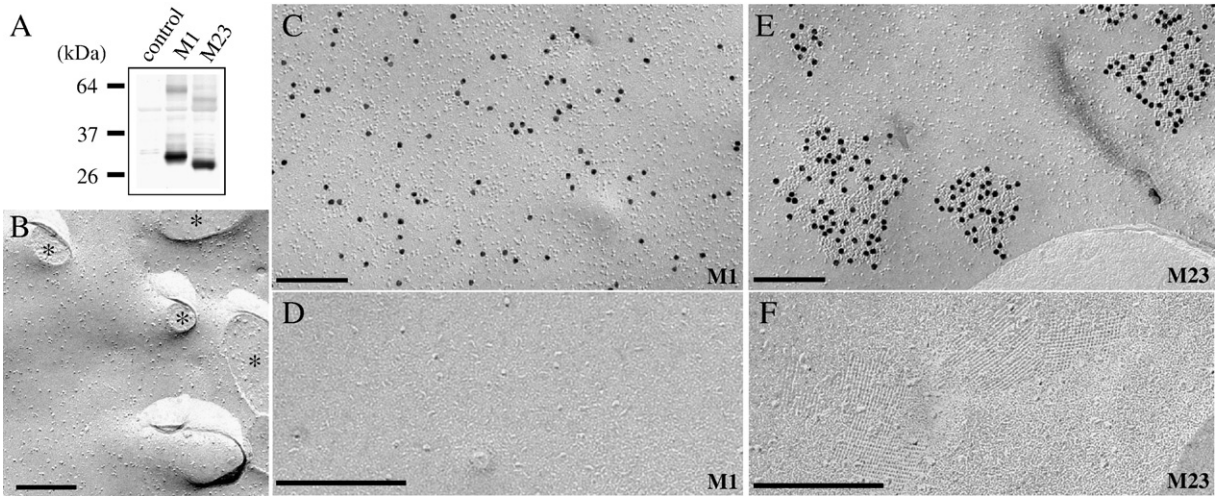

Fig. 1. Expression of ratAQP4 isoforms in CHO cells and SDS-FRL analysis. (A) Immunoblot of lysates of CHO cells transfected with AQP4M1, AQP4M23 or no vector (control), probed with anti-AQP4CT antibody. The major bands are at the expected positions for the two AQP4 isoforms, while the minor bands would correspond to dimers of the respective isoforms. (B) No immunolabeling is observed on the P-face of non-transfected CHO cells by SDS-FRL. Asterisks indicate cross-fractured regions through protruding portions of the cells. (C and D) SDS-FRL images of the P-face (C) and the E-face (D) of CHO cells transfected with AQP4M1. Immunogold particles are evenly distributed over the P-face, whereas the E-face shows the absence of square arrays and immunogold particles. (E and F) SDS-FRL images of the P-face (E) and the E-face (F) of CHO cells transfected with AQP4M23. Immunogold particles on the P-face are exclusively found on the square arrays. The E-face shows pit-like imprints of the square arrays. The smooth, featureless area shows the buffer region outside the cells. Scale bars are 200 nm.

2.5. Fixation

Mild fixation of the cells with 2% formaldehyde for 30 min resulted in deformation of the square arrays on the protoplasmic fracture face (P-face) and the deposition of IMPs on the square array pits on the exoplasmic fracture face (E-face). This suggested that inappropriate fixation conditions caused AQP4 molecules in square arrays to distribute randomly between the P-and E-faces. Fixation with 2.5% glutaraldehyde showed similar morphology of the square arrays to those obtained by overnight fixation with 4% formaldehyde at 37 °C (data not shown), but glutaraldehyde fix is not suitable for SDS-FRL. To observe the square arrays by SDS-FRL, it was thus essential to fix the cells overnight with 4% formaldehyde at 37 °C. The antigenicity of AQP4 was preserved under these fixation conditions.

2.6. Electron microscopy

Replica specimens were imaged in a JEM-1010 electron microscope (JEOL, Tokyo, Japan) equipped with a 2K slow-scan CCD camera (Gatan, Warrendale, PA, USA) at a magnification of 15,000–40,000×. Images were analyzed with ImageJ (NIH). To qualify as square arrays, IMP assemblies had to have at least four IMPs on each side. Because gold particles can be removed from epitopes by 20–30 nm due to the size of the antibody [25], gold particles within 30 nm of an edge of a square array were considered to recognize AQP4 in square arrays.

2.7. Acyl-Biotinyl Exchange (ABE) Chemistry

The ABE procedure was modified from the original reports [26,27] in the following way. Transfected CHO cells were harvested 24 h after transfection, and the cell pellets were resuspended in homogenization buffer (20 mM Tris–HCl, pH 7.5, 150 mM NaCl, 5 mM EDTA) containing 10 mM *N*-ethyl maleimide (NEM; freshly prepared) and a protease inhibitor cocktail (Nakalai Tesque, Kyoto, Japan). Membrane fractions were obtained by disrupting cells in a Potter-Elvehjem homogenizer on ice, and cell debris was removed by centrifugation at 1000 ×*g* for 10 min. After another centrifugation at 40,000 ×*g* for 30 min, pellets were resuspended in solubilization buffer (SB: 1% Triton X-100 in 20 mM Tris–HCl, pH 7.5, 150 mM NaCl) containing 10 mM NEM and incubated for 30 min on ice. After centrifugation at 100,000 ×*g* for 60 min, the supernatants were incubated overnight at 4 °C with affinity resin that was prepared by using dimethyl pimelimidate (PIERCE) to cross-link anti-AQP4CT antibody to Protein G Sepharose (GE Healthcare). After removal of NEM by three washes with SB, the resin was divided into two aliquots. One aliquot was incubated with 1 M hydroxylamine (pH 7.5) in 150 mM NaCl, 1% Triton X-100 and 1 mM iodoactyl-PEO_2-Biotin (PIERCE) for 1 h at room temperature. The other aliquot served as control and was incubated with 1 M Tris–HCl (pH 7.5) in the same buffer. After three washes with SB, bound proteins were eluted with 100 mM glycine–HCl buffer (pH 2.7) containing 1% Triton X-100. The samples were analyzed by SDS-PAGE and Western blotting using both streptavidin alkaline phosphatase (avidin-AP) (Promega) and anti-AQP4CT antibody. For immunoprecipitation and ABE chemistry of AQP4 from brain tissue, a cerebellum was dissected from

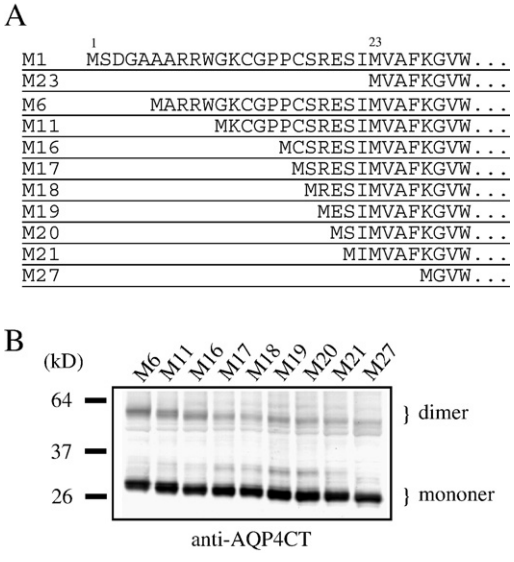

Fig. 2. N-terminal deletion mutants of AQP4. (A) Amino acid sequences of the N-termini of AQP4M1, AQP4M23 and mutants with increasingly long N-terminal deletions. The number of the mutant indicates the position of the initiation methionine relative to AQP4M1. (B) Immunoblot of lysates of CHO cells transfected with the various N-terminal deletion mutants of AQP4, probed with anti-AQP4CT antibody. The same amounts of cell lysates from 35-mm dish cultures were loaded on the SDS-PAGE gel.

an adult rat brain (Funakoshi, Tokyo, Japan) and homogenized in a Potter-Elvehjem homogenizer on ice with homogenization buffer (7.5 mM sodium phosphate, pH 7.2, 250 mM sucrose, 5 mM EDTA) containing a protease inhibitor cocktail. The subsequent procedure was the same as that for the CHO cells.

2.8. Metabolic labeling

16 h after transfection CHO cells plated in 60-mm dishes were preincubated for 30 min in serum-free DMEM containing 10 mg/ml fat-free bovine serum albumin (SIGMA). [^{3}H]-palmitic acid in ethanol was concentrated in a vacuum centrifuge so that the final ethanol volume was 1% of the labeling medium. Cells were labeled with 9.25 MBq/ml [^{3}H]-palmitic acid for 4 h in preincubation medium. Cells were harvested and extracted on ice for 30 min with SB containing a protease inhibitor cocktail. After centrifugation at 14,000 ×*g* for 10 min, the supernatants were incubated with anti-AQP4CT antibody overnight at 4 °C. Protein G sepharose was added to the samples, and after a 1-hour incubation at 4 °C, the resin was washed with SB. Bound proteins were eluted with SDS-PAGE sample buffer for 10 min at room temperature and analyzed by SDS-PAGE. For fluorography, gels were immersed in a fixing solution (25% isopropanol, 10% acetic acid, 65% H_2O) for 30 min, treated with Amplify (GE Healthcare) for 30 min, dried under vacuum and exposed to BioMax MS film (Kodak) for 2 weeks at −80 °C.

3. Results

3.1. Expression of WT AQP4 and SDS-FRL

The WT *aqp4* gene has two translation initiation codons, encoding methionine residues Met1 and Met23, so that *in vivo* two AQP4 isoforms are expressed, AQP4M1 and AQP4M23. To analyze the formation of square arrays *in vitro*, we cloned AQP4M1 and AQP4M23 full-length cDNAs into mammalian expression vectors. Expression of the two WT AQP4 isoforms in transfected CHO cells was confirmed by immunoblotting (Fig. 1A). An antibody against the C-terminus of AQP4 (anti-AQP4CT) detected protein bands with apparent molecular weights of 30 kDa and 28 kDa in the solubilized cell lysates,

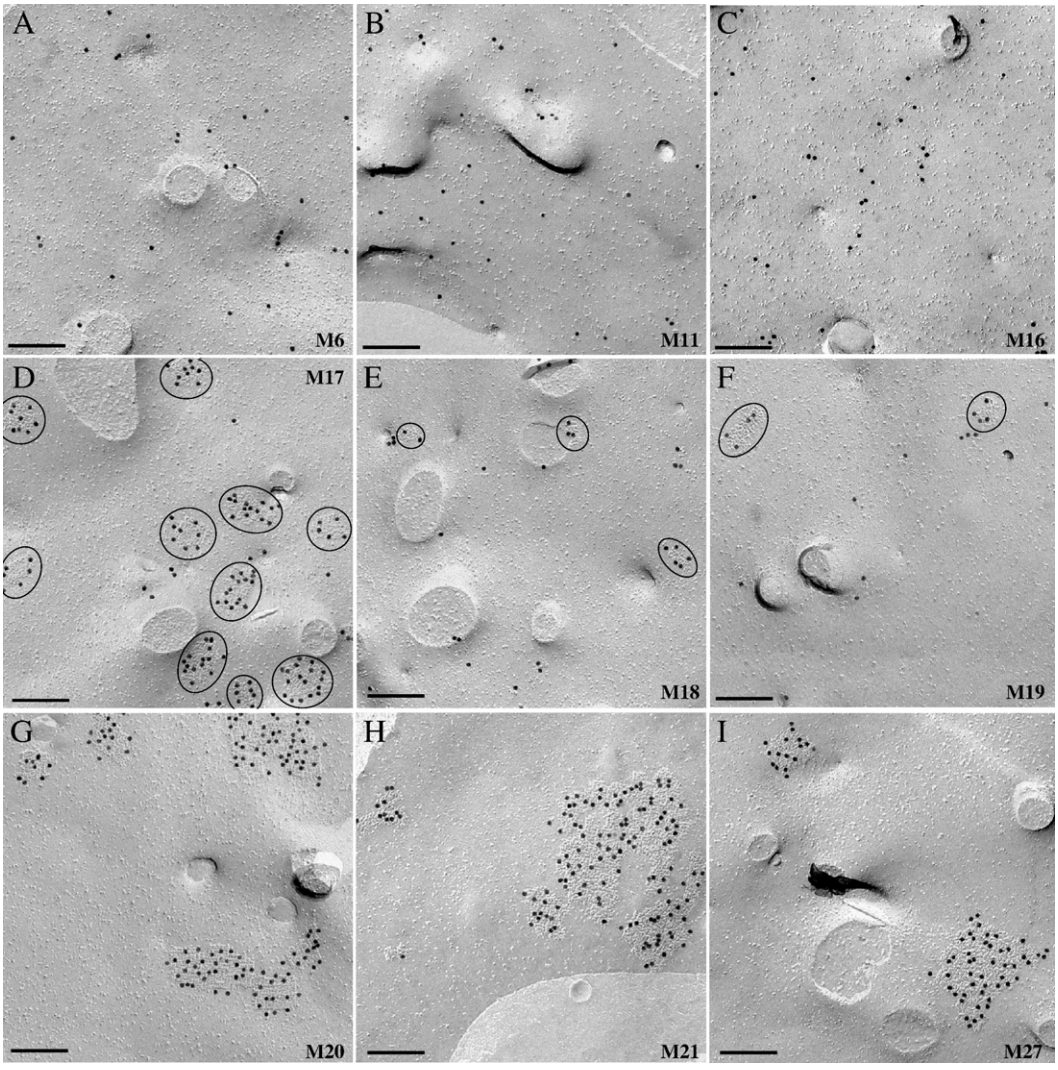

Fig. 3. Representative P-face images of plasma membranes of CHO cells transiently expressing various N-terminal deletion mutants. All replicas were analyzed by SDS-FRL. (A–C) No square arrays were observed with CHO cells expressing the M6 (A), M11 (B) and M16 (C) mutants. Almost all immunogold particles were evenly distributed over the entire plasma membranes. (D–F) Square arrays (circles) were observed with CHO cells expressing the M17 (D), M18 (E) and M19 (F) mutants. Some gold particles labeled square arrays, while others were found outside of the arrays. (G) For CHO cells expressing the M20 mutant, almost all gold particles labeled the square arrays. (H and I) For CHO cells expressing the M21 (H) and M27 (I) mutants, all gold particles were associated with square arrays. Scale bars are 200 nm.

consistent with the two AQP4 isoforms. We then analyzed CHO cells transiently expressing AQP4M1 or AQP4M23 by SDS-FRL using anti-AQP4CT as the first antibody and a 15-nm gold conjugated secondary antibody. Since the C-terminus, which is recognized by anti-AQP4CT, is exposed on the cytoplasmic side, specific immunogold labeling should only be observed on the P-face of the plasma membrane. We confirmed that no labeling was detected with non-transfected CHO cells (Fig. 1B). When the AQP4M1 isoform of AQP4 was expressed in CHO cells, both IMPs and immunogold labels were evenly dispersed on the P-face (Fig. 1C). The E-face showed a concave shape, a lower density of IMPs than the P-face (Fig. 1D), which is commonly seen for biological membranes, and no immunogold labels. By contrast, when the shorter AQP4M23 isoform was expressed in CHO cells, square arrays of IMPs were observed on the P-faces, which were specifically labeled with a high density of immunogold particles (Fig. 1E). Images of the E-faces revealed the complementary pits of the square array particles (Fig. 1F) but no immunogold particles. While the pit-like imprints of the arrays on the E-faces showed that the square arrays were well ordered, the IMP arrays seen on the P-faces showed much less order. This observation indicates that the native arrays are indeed very well ordered and that the loss of order of the IMP arrays seen on the P-faces is due to the splitting of the membrane during the freeze fracture procedure. The size of the square arrays seen on cells transfected with AQP4M23 varied from ~1500 nm^2 to ~70,000 nm^2 due to variations in the expression level between cells transiently expressing AQP4M23. We also established CHO cell lines stably expressing AQP4M1 and AQP4M23. As with the transient expressions, AQP4M23 cell lines showed the square arrays whereas AQP4M1 expressing cell lines did not (data not shown). In the following freeze fracture studies, we used the transient expression system and used SDS-FRL to confirm the expression of AQP4.

3.2. Construction and expression of AQP4 mutants with N-terminal deletions

To identify the regions in the N-terminus that affect the formation of AQP4 square arrays, we constructed a series of N-terminal deletion mutants (Fig. 2A). It should be noted that the M6 construct, for example, lacked the six N-terminal residues of the AQP4M1 sequence but contained an additional initiation methionine. All AQP4 deletion mutants were expressed in transfected cells as determined by immunoblotting of cell lysates (Fig. 2B), and their correct localization to the plasma membrane was confirmed by SDS-FRL (Fig. 3A–I).

3.3. SDS-FRL of CHO cells transfected with N-terminal deletion mutants

When the M6, M11 or M16 constructs were expressed in CHO cells, no square arrays were observed and the gold labels were evenly dispersed over the P-faces of the plasma membranes (Fig. 3A–C). By contrast, N-terminal deletion mutants that were shorter than the M16 construct showed square arrays with different characteristics. In the case of M17, many of immunogold particles labeled the square arrays, but some of gold labels could also be seen outside the square arrays (Fig. 3D). This implies that the mutant AQP4 molecules are inclined to assemble into square arrays but some of the molecules are detached from the arrays. To estimate the percentage of AQP4 molecules in square arrays, we counted the number of gold labels on square arrays and compared it with the number of all gold labels on the P-faces in each image. The mean percentages and standard deviations (SD) of the labeling in the WT and mutant AQP4s were graphed in Fig. 4. In the case of AQP4M1, 0%±0% (mean±SD; $n=10$) of the gold particles were found on square arrays, whereas for AQP4M23, 95%±5% ($n=7$) of the gold particles were localized on square arrays. The M16 mutant (0%±0%; $n=6$) behaved like AQP4M1, but in the case of the M17 mutant, 67%±22% ($n=10$) of the gold particles localized to square arrays, demonstrating that this construct can form square arrays although less efficiently than AQP4M23. The M18 mutant showed a lower frequency of labeled square arrays, while most of the gold labels were randomly dispersed over the P-faces (12%±18%; $n=10$) (Fig. 3E), and a similar distribution of the gold particles was observed for the M19 mutant (21%±18%; $n=10$) (Fig. 3F). The M20 mutant showed prominent square arrays, but the percentage of gold labels on the arrays substantially varied between cells (83%±21%; $n=10$) (Fig. 3G). As shown by the standard deviations for M17–M20, the frequency of square array formation and the percentage of gold labels on square arrays varied between different cells and fields of view. The variance in the assembly of AQP4 into square arrays did, however, not correlate with the expression levels of the AQP4 mutants. In contrast to mutants M17–M20, the assembly of M21 (96%±5%; $n=8$) (Fig. 3H) into square arrays was indistinguishable from AQP4M23. Finally, the M27 mutant (96%±4%; $n=9$) (Fig. 3I), which lacks most of the cytoplasmic N-terminal tail of AQP4 whose first transmembrane domain starts with Trp30 [18], also formed square arrays with the same efficiency as AQP4M23. Although the reason for the variations seen in the M17–M20 mutants in the percentage of AQP4 molecules assembling into square arrays is currently

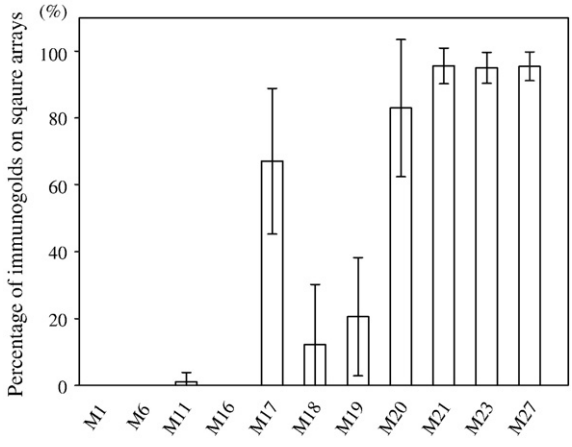

Fig. 4. WT and deletion mutant AQP4 constructs show different propensities for square array formation. Bars indicate the mean percentages of the immunogold labels on square arrays. The numbers of gold particles on square arrays were divided by the numbers of all gold particles on the P-face in each observed field. Error bars are ±SD.

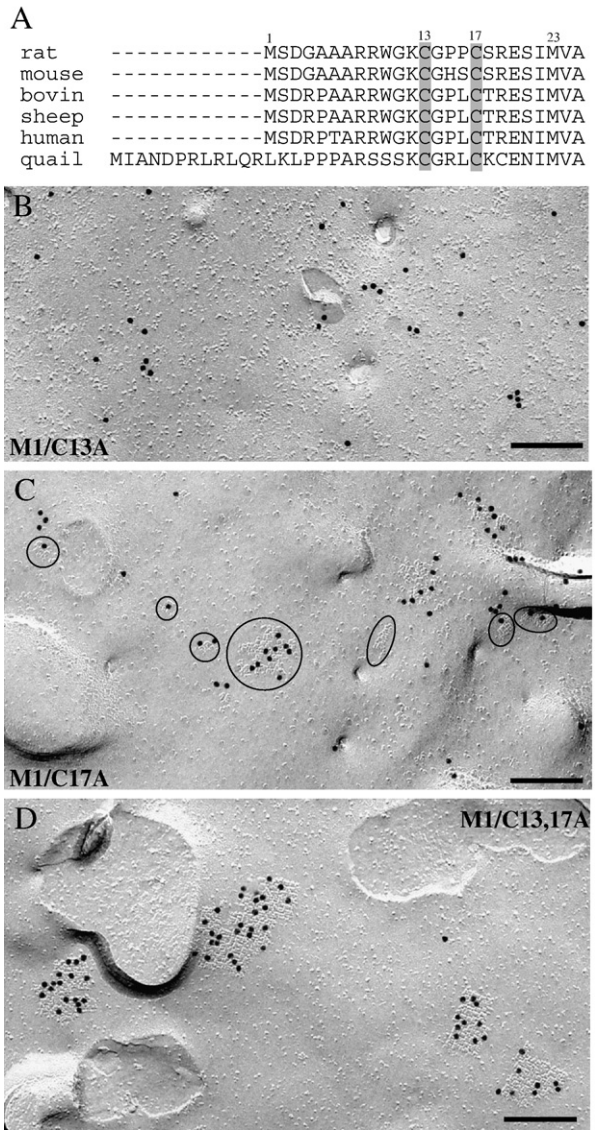

Fig. 5. Cysteine substitutions in the N-terminus of full-length AQP4M1 and SDS-FRL analysis. (A) Alignment of the N-terminal amino acid sequences of AQP4 from different species, showing that the cysteine residues at positions 13 and 17 are conserved. (B–D) Representative P-face images of plasma membranes of CHO cells transiently expressing AQP4M1 mutants in which one or both cysteines were substituted by alanine. All replicas were analyzed by SDS-FRL. (B) CHO cells expressing the single cysteine mutant AQP4M1/C13A showed no square arrays. (C) CHO cells expressing the other single cysteine mutant AQP4M1/C17A showed occasional square arrays (circles). (D) CHO cells expressing the double cysteine mutant AQP4M1/C13,17A revealed that almost all gold labels localized to square arrays. Scale bars are 200 nm.

unclear, there was a distinct difference between the M16 and M17 mutants in terms of their abilities to form square arrays. These results suggest that disruption of array formation is either caused by an N-terminus longer than that of the M17 mutant and/or by specific amino acids in the region from Cys17 to Ser21 (Cys-Ser-Arg-Glu-Ser).

3.4. Cysteine substitutions in AQP4M1 and SDS-FRL

The cysteine residues at positions 13 and 17 of rat AQP4M1 are conserved in homologs from different species (Fig. 5A), and the M17 mutant lacked both of these cysteines. To verify the possible involvement of Cys13 and/or Cys17 in interfering with the formation of square arrays, we generated AQP4M1 mutants, in which either one or both cysteine residues were mutated to alanine. CHO cells transfected with these mutant constructs were analyzed by SDS-FRL. Electron microscopy showed that the single cysteine mutant AQP4M1/C13A formed no square arrays while the other single cysteine mutant, AQP4M1/C17A, formed a few, small arrays (Fig. 5B and C), respectively. By contrast, the double cysteine mutant, AQP4M1/C13,17A, formed square arrays very efficiently (Fig. 5D). These observations were confirmed by quantifying the percentages of gold particles on square arrays, which were 93%±10% for AQP4M1/C13,17A (n=7), but only 0%±0% for AQP4M1/C13A (n=10) and 27%±29% for AQP4M1/M17A (n=9). These results indicate that the presence of even only one of the two cysteine residues suffices to disrupt the formation of square arrays.

3.5. The N-terminal cysteines of AQP4M1 are palmitoylated in CHO cells

Cysteine residues can serve as sites for posttranslational modifications by fatty acids, but AQP4M1 lacks classical consensus sequences for both N-terminal myristoylation and C-terminal prenylation [28,29]. Palmitoylation, another lipid modification of cysteines, often occurs at the N-terminus of proteins without well-defined consensus sequences [30]. To test the possibility that the N-terminal cysteines in AQP4 are palmitoylated, we immunoprecipitated AQP4 from transfected

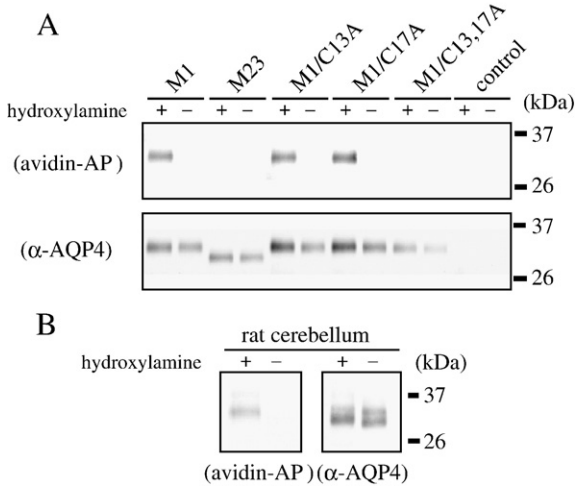

Fig. 6. (A) AQP4M1, AQP4M23, AQP4M1/C13A, AQP4M1/C17A or AQP4M1/C13,17A were expressed in CHO cells, immunoprecipitated and subjected to ABE chemistry [27]. Non-transfected CHO cells were used as control. Cells were homogenized, fractionated, solubilized and immunoprecipitated in the presence of 10 mM NEM. The immunoprecipitates were bound to affinity resin, washed without NEM and treated with sulfydryl-reactive biotinylation regent in the presence or absence of hydroxylamine. The eluates were analyzed on Western blots, which were probed with avidin-AP to detect biotinylated proteins (upper panel) or anti-AQP4CT antibody (lower panel) to verify the presence of the various AQP4 constructs. (B) The intrinsic AQP4 was immunoprecipitated from an adult rat cerebellum and subjected to the same ABE procedure.

CHO cell lysates using anit-AQP4CT antibody and analyzed the immunoprecipitates using acyl-biotinyl exchange (ABE) chemistry [26,27]. In the ABE approach three sequential chemical steps are performed to convert palmitoylated proteins to biotinylated proteins, which can then be identified with high sensitivity. First, the free thiol groups are alkylated by NEM, followed by hydroxylamine cleavage of thioester bonds that link the fatty acids to the proteins. Finally, the newly exposed free thiols are biotinylated with thiol-specific biotinylation regents. As shown in the upper panel of Fig. 6A, biotinylations were detected for AQP4M1, AQP4M1/C13A and AQP4M1/C17A, but not for AQP4M23 or AQP4M1/C13,17A. The presence of the various AQP4 constructs in the immunoprecipitates was confirmed by immunoblotting with anit-AQP4CT antibody (Fig. 6A; lower panel). These results show that both Cys13 and Cys17 carry posttranslational modifications through thioester bonds. For elucidating whether lipid modification actually occurs in AQP4M1 *in vivo*, we immunoprecipitated AQP4 from the lysate of rat cerebellum and performed the ABE chemistry. The immunoblot showed two bands of AQP4 corresponding to the M1 and M23 isoforms, and the biotinylation signal was detected at the position of M1 with hydroxylamine treatment (Fig. 6B). This indicates that AQP4M1 can be posttranslationally modified in the brain as well as in CHO cells. To determine whether AQP4M1 expressed in CHO cells is indeed palmitoylated, we performed metabolic labeling with [^{3}H]-palmitic acid. Fig. 7A shows a fluorograph of solubilized AQP4 constructs purified by anti-AQP4CT precipitation. The corresponding silver-stained gel shows 30-kDa or 28-kDa bands, verifying that each construct was present in the immunoprecipitates (Fig. 7B). The fluorograph revealed the corresponding 30-kDa bands only in the samples containing AQP4M1, AQP4M1/C13A and AQP4M1/C17A. Signals were also found at the dye fronts and the top of the lanes, as is commonly seen in fluorography with [^{3}H]-palmitic acid [31]. Quantification of the band intensities by densitometry showed that the intensity of the 30-kDa band in the AQP4M1 sample was almost twice as high as those of the bands in the AQP4M1/C13A and the AQP4M1/C17A samples. These results thus reveal that in AQP4M1 expressed in CHO cells both Cys13 and Cys17 are palmitoylated.

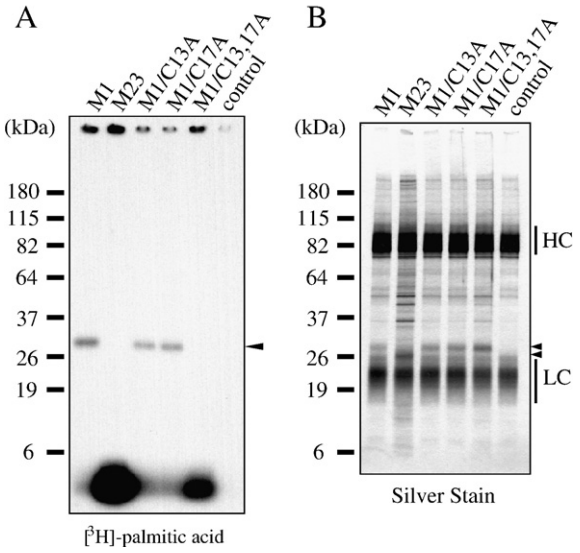

Fig. 7. Metabolic labeling of CHO cells expressing AQP4 constructs. (A) CHO cells were metabolically labeled with [^{3}H]-palmitic acid and the lysates were immunoprecipitated with anti-AQP4CT antibody. The fluorography demonstrates that AQP4M1, AQP4M1/C13A and AQP4M1/C17A are palmitoylated (arrowhead). Signals at the dye fronts and top of the lanes indicate non-specific contamination with free [^{3}H]-palmitic acid. (B) The silver stained gel of the same samples shown in (A) confirms the presence of the various AQP4 cysteine mutants in the immunoprecipitates (arrowheads). The strong bands at molecular weights of about 90 kDa and 20 kDa represent the heavy chains (HC) and light chains (LC) of the polyclonal IgG antibody.

4. Discussion

Previous studies established that the two alternative splice variants of AQP4 have opposing effects on the formation of square arrays [16,17]. Since the two AQP4 isoforms differ only in the length of their N-termini, this should be the region that affects array formation. In this study, we used freeze fracture electron microscopy of CHO cells transfected with mutant AQP4s to identify the N-terminal residues that regulate the formation of square arrays.

The systematic deletion of residues in the N-terminus of AQP4M1 showed that mutants with deletions of less than seventeen residues behaved like AQP4M1 and did not form square arrays. The propensity to form square arrays increased dramatically for the M17 mutant. This finding indicated that array formation is inhibited either by too long an N-terminus and/or by Cys17, which was present in the M16 mutant but lacking in the M17 construct. The possibility of steric hindrance due to the mere bulk of the additional N-terminal residues in AQP4M1 was unlikely to be the cause for its failure to form arrays, because an additional N-terminal tag of 35 amino acids did not affect the two-dimensional crystallization of recombinant AQP4M23 [18]. We therefore examined the influence of the two N-terminal cysteine residues of AQP4M1 on array formation without changing the length of the N-terminus. The AQP4 double mutant, in which both cysteines were replaced by alanines, was very efficient in forming square arrays in CHO cells. However, although the cysteines at positions 13 and 17 clearly have a dramatic effect on array formation, it is unclear why the M18 and M19 mutants, which are also lacking both N-terminal cysteines, were not efficient in forming square arrays. Similarly, it is also not clear why the M20 mutant was not as efficient in array formation as AQP4M23. As shown in Fig. 4, all the M17, M18, M19 and M20 showed fluctuated propensities for the formation of square arrays. The variations seen in these AQP4 deletion mutants may imply that, rather than one single amino acid residue, the truncated N-terminus partially containing the region from Ser18 to Ser21 could be involved in the interference with the close packing of the AQP4 tetramers due to the artificial N-terminal length or the other unidentified factors.

The M27 construct whose N-terminus is shorter than that of AQP4M23 did form square arrays. Since this mutant lacks most of the cytosolic N-terminal residues and the remaining three residues extending from the first transmembrane domain would

most likely not be able to make significant interactions with neighboring tetramers, this result suggests that the N-terminus itself is not directly involved in interactions that stabilize the square arrays. This conclusion is consistent with the notion that square arrays are formed by interactions between the transmembrane regions of neighboring AQP4 tetramers [18].

The appearance of square arrays in the AQP4M1/C13,17A double mutant indicates that the cysteines are the critical residues that interfere with array formation. Between the two cysteines are two proline residues at positions 15 and 16 (Fig. 5A), which would make this N-terminal region rather flexible, suggesting that it is not the presence of a rigid domain that interferes with array formation. Cysteine-directed protein modification was an alternative possibility how the two cysteines could prevent array formation. ABE chemistry and metabolic labeling with palmitic acid showed that both Cys13 and Cys17 were palmitoylated when AQP4M1 was expressed in CHO cells. AQP4M1 contains a total of eight cysteine residues, two in the N-terminus, five scattered throughout the transmembrane helices and one in the C-terminus, adjacent to the sixth transmembrane domain. Since no palmitic acid signal was observed with the AQP4M1/C13,17A double mutant, the two N-terminal cysteines are the only palmitoylation sites in AQP4. As is the case for AQP4, palmitoylation often occurs at cysteine residues up to 20 amino acids from the N-terminus [32], close to basic and hydrophobic residues [33]. For most transmembrane proteins, however, such as G-protein coupled receptors [30], AMPA receptors [34], and synaptotagmin [35], palmitoylation occurs at cytosolic cysteines at the roots of intracellular loops and/or just downstream of the last transmembrane domain [33]. Only very few transmembrane proteins, one example would be tetraspanin CD151 [36], have been reported to be N-terminally palmitoylated like AQP4.

In AQP4M1, the double cysteine substitution resulted in the loss of palmitoylation and simultaneously the mutant became efficient in forming square arrays. These results suggest that the N-terminal palmitoylation is a crucial factor in preventing AQP4M1 to form square arrays. Palmitoylation of cysteine residues typically facilitates the interactions of proteins with the lipid membrane and modulates their functions [30,33]. Our previously determined density map of AQP4M23 suggested that the N-terminus is located close to the area where four adjacent tetramers come together in the square arrays [18]. Attachment of the N-terminus to the lipid bilayer by palmitoylation could thus cause steric hindrances that would prevent AQP4M1 tetramers to come close enough to each other to form an array. This mechanism would constitute an unprecedented function of palmitoylation in the regulation of interactions between membrane proteins. However we cannot conclude that the palmitoylation is the sole determinant for the destabilization of the square arrays, because we could so far get less clear results in our attempt to confirm the direct effect for the array disruption by the palmitoylation itself while leaving the two cysteines in place. In our preliminary experiments of the AQPM1 transfected cells, the effect of 2-bromopalmitate, an inhibitor that blocks palmitate incorporation into proteins [37], could not give clear arrays while some aggregation of IMPs on the P-faces and small pit-type arrays on the E-faces were observed (data not shown). Therefore, much more studies for the complete inhibition of palmitoylation are required. These experimental results together with fluctuated propensities of the array formation by the mutants of M17, M18, M19 and M20 as shown in Fig. 4 suggested that the other unknown factors in the N-terminus of AQP4M1 could not be excluded, although N-terminal palmitoylation is the crucial determinant for the array deformation.

It should be noted that the formation of square arrays may be regulated by more than one mechanism, because palmitoylation is labile and reversible depending on cellular conditions and physiological signaling. The expression ratio of AQP4M1 and AQP4M23 would also determine the potential of AQP4 to be palmitoylated. Differential palmitoylation due to alternative splicing has been reported for some cytosolic proteins in neurons [38–40], altering their auxiliary functions and trafficking to the plasma membrane. AMPA receptors have two palmitoylation sites, one in the second transmembrane domain and one in the C-terminal region, and the palmitoylation state may modulate the trafficking of these receptors [34,41]. In the case of AQP4, there is no evidence that AQP4M1 and AQP4M23 are trafficked differently, and the polarized anchoring of AQP4 to astrocyte endfeet is likely due to its C-terminal PDZ binding domain [6,15]. However, the extent and dynamics of palmitoylation of AQP4M1 *in vivo* is unknown. It may thus be that AQP4M1 in the plasma membrane is not palmitoylated, and regulated palmitoylation of AQP4M1 could then be a mechanism to disrupt square arrays. This model could explain how square arrays can be rapidly disassembled after circulatory arrest [13]. It cannot be excluded, however, that *in vivo* square arrays contain a certain amount of palmitoylated AQP4M1, which could then play a role in providing suitable sizes of the arrays for rapid disassembly by the other mechanisms, as previously proposed [16]. In this case, palmitoylation may function as a sorting signal of AQP4M1/AQP4M23 heterotetramer clusters to specific membrane domains, as has been reported for PSD-95 and GAP-43 [42], or to the membrane microdomains such as lipid rafts.

Although our studies remain uncertain whether palmitoylation actually occurs *in vivo* and at the same Cys13 and Cys17 as in CHO cells, the biochemical analyses of the brain tissue by ABE chemistry showed that some kind of fatty acylation of the AQP4 occurred also *in vivo*, implying the possibility that some extent of palmitoylated AQP4 is present in the brain (Fig. 6B). Further studies are needed to test the hypotheses described above and to relate the palmitoylation state of AQP4 *in vivo* with morphological and functional differences between the two AQP4 isoforms. The palmitoylation of AQP4 is the first finding of lipid modification on water channels, and encourages further studies for establishing whether other water channels also contain lipid modifications.

Acknowledgments

The authors acknowledge Dr. Sei Sasaki for the gift of original cDNA for this study. The authors also thank Drs. Ryuichi Shigemoto, Yugo Fukazawa, Shinpei Yamaguchi, Kazutoshi Tani and Tomoko Doi for scientific advice and technical assistance. We acknowledge Dr. Thomas Walz for critical reading of

the manuscript. This research was supported by Grants-in-Aid for Specially Promoted Research, the Japan New Energy and Industrial Technology Development Organization (NEDO) and the Global Center of Excellence Program "Formation of a Strategic Base for Biodiversity and Evolutionary Research: from Genome to Ecosystem" of the Ministry of Education, Culture, Sports and Technology (MEXT), Japan.

References

[1] M. Borgnia, S. Nielsen, A. Engel, P. Agre, Cellular and molecular biology of the aquaporin water channels, Annu. Rev. Biochem. 68 (1999) 425–458.
[2] K. Murata, K. Mitsuoka, T. Hirai, T. Walz, P. Agre, J.B. Heymann, A. Engel, Y. Fujiyoshi, Structural determinants of water permeation through aquaporin-1, Nature 407 (2000) 599–605.
[3] T. Gonen, T. Walz, The structure of aquaporins, Q. Rev. Biophys. 39 (2006) 361–396.
[4] S. Nielsen, J. Frøkiaer, D. Marples, T.H. Kwon, P. Agre, M.A. Knepper, Aquaporins in the kidney: from molecules to medicine, Physiol. Rev. 82 (2002) 205–244.
[5] S. Nielsen, E.A. Nagelhus, M. Amiry-Moghaddam, C. Bourque, P. Agre, O.P. Ottersen, Specialized membrane domains for water transport in glial cells: high-resolution immunogold cytochemistry of aquaporin-4 in rat brain, J. Neurosci. 17 (1997) 171–180.
[6] J.D. Neely, M. Amiry-Moghaddam, O.P. Ottersen, S.C. Froehner, P. Agre, M.E. Adams, Syntrophin-dependent expression and localization of Aquaporin-4 water channel protein, Proc. Natl. Acad. Sci. U. S. A. 98 (2001) 14108–14113.
[7] G.T. Manley, M. Fujimura, T. Ma, N. Noshita, F. Filiz, A.W. Bollen, P. Chan, A.S. Verkman, Aquaporin-4 deletion in mice reduces brain edema after acute water intoxication and ischemic stroke, Nat. Med. 6 (2000) 159–163.
[8] M. Amiry-Moghaddam, O.P. Ottersen, The molecular basis of water transport in the brain, Nat. Rev., Neurosci. 4 (2003) 991–1001.
[9] D.M. Landis, T.S. Reese, Arrays of particles in freeze-fractured astrocytic membranes, J. Cell Biol. 60 (1974) 316–320.
[10] L. Orci, F. Humbert, D. Brown, A. Perrelet, Membrane ultrastructure in urinary tubules, Int. Rev. Cytol. 73 (1981) 183–242.
[11] J.E. Rash, L.A. Staehelin, M.H. Ellisman, Rectangular arrays of particles on freeze-cleaved plasma membranes are not gap junctions, Exp. Cell Res. 86 (1974) 187–190.
[12] J.E. Rash, T. Yasumura, C.S. Hudson, P. Agre, S. Nielsen, Direct immunogold labeling of aquaporin-4 in square arrays of astrocyte and ependymocyte plasma membranes in rat brain and spinal cord, Proc. Natl. Acad. Sci. U. S. A. 95 (1998) 11981–11986.
[13] D.M. Landis, T.S. Reese, Astrocyte membrane structure: changes after circulatory arrest, J. Cell Biol. 88 (1981) 660–663.
[14] J.S. Jung, R.V. Bhat, G.M. Preston, W.B. Guggino, J.M. Baraban, P. Agre, Molecular characterization of an aquaporin cDNA from brain: candidate osmoreceptor and regulator of water balance, Proc. Natl. Acad. Sci. U. S. A. 91 (1994) 13052–13056.
[15] J.D. Neely, B.M. Christensen, S. Nielsen, P. Agre, Heterotetrameric composition of aquaporin-4 water channels, Biochemistry 38 (1999) 11156–11163.
[16] C.S. Furman, D.A. Gorelick-Feldman, K.G. Davidson, T. Yasumura, J.D. Neely, P. Agre, J.E. Rash, Aquaporin-4 square array assembly: opposing actions of M1 and M23 isoforms, Proc. Natl. Acad. Sci. U. S. A. 100 (2003) 13609–13614.
[17] C. Silberstein, R. Bouley, Y. Huang, P. Fang, N. Pastor-Soler, D. Brown, A.N. Van Hoek, Membrane organization and function of M1 and M23 isoforms of aquaporin-4 in epithelial cells, Am. J. Physiol. Renal Physiol. 287 (2004) F501–F511.
[18] Y. Hiroaki, K. Tani, A. Kamegawa, N. Gyobu, K. Nishikawa, H. Suzuki, T. Walz, S. Sasaki, K. Mitsuoka, K. Kimura, A. Mizoguchi, Y. Fujiyoshi, Implications of the Aquaporin-4 structure on array formation and cell adhesion, J. Mol. Biol. 355 (2006) 628–639.
[19] T. Gonen, Y. Cheng, P. Sliz, Y. Hiroaki, Y. Fujiyoshi, S.C. Harrison, T. Walz, Lipid–protein interactions in double-layered two-dimensional AQP0 crystals, Nature 438 (2005) 633–638.
[20] N. Buzhynskyy, J.F. Girmens, W. Faigle, S. Scheuring, Human cataract lens membrane at subnanometer resolution, J. Mol. Biol. 374 (2007) 162–169.
[21] N. Buzhynskyy, R.K. Hite, T. Walz, S. Scheuring, The supramolecular architecture of junctional microdomains in native lens membranes, EMBO Rep. 8 (2007) 51–55.
[22] S. Scheuring, N. Buzhynskyy, S. Jaroslawski, R.P. Gonçalves, R.K. Hite, T. Walz, Structural models of the supramolecular organization of AQP0 and connexons in junctional microdomains, J. Struct. Biol. 160 (2007) 385–394.
[23] K. Fujimoto, Freeze-fracture replica electron microscopy combined with SDS digestion for cytochemical labeling of integral membrane proteins. Application to the immunogold labeling of intercellular junctional complexes, J. Cell Sci. 108 (1995) 3443–3449.
[24] M. Masugi-Tokita, E. Tarusawa, M. Watanabe, E. Molnár, K. Fujimoto, R. Shigemoto, Number and density of AMPA receptors in individual synapses in the rat cerebellum as revealed by SDS-digested freeze-fracture replica labeling, J. Neurosci. 27 (2007) 2135–2144.
[25] K. Fujimoto, SDS-digested freeze-fracture replica labeling electron microscopy to study the two-dimensional distribution of integral membrane proteins and phospholipids in biomembranes: practical procedure, interpretation and application, Histochem. Cell Biol. 107 (1997) 87–96.
[26] A.F. Roth, J. Wan, A.O. Bailey, B. Sun, J.A. Kuchar, W.N. Green, B.S. Phinney, J.R. Yates, N.G. Davis, Global analysis of protein palmitoylation in yeast, Cell 125 (2006) 1003–1013.
[27] R.C. Drisdel, J.K. Alexander, A. Sayeed, W.N. Green, Assays of protein palmitoylation, Methods 40 (2006) 127–134.
[28] D.R. Johnson, R.S. Bhatnagar, L.J. Knoll, J.I. Gordon, Genetic and biochemical studies of protein *N*-myristoylation, Annu. Rev. Biochem. 63 (1994) 869–914.
[29] F.L. Zhang, P.J. Casey, Protein prenylation: molecular mechanisms and functional consequences, Annu. Rev. Biochem. 65 (1996) 241–269.
[30] J.E. Smotrys, M.E. Linder, Palmitoylation of intracellular signaling proteins: regulation and function, Annu. Rev. Biochem. 73 (2004) 559–587.
[31] T. Doi, H. Sugimoto, I. Arimoto, Y. Hiroaki, Y. Fujiyoshi, Interactions of endothelin receptor subtypes A and B with Gi, Go, and Gq in reconstituted phospholipid vesicles, Biochemistry 38 (1999) 3090–3099.
[32] I. Navarro-Lérida, A. Alvarez-Barrientos, F. Gavilanes, I. Rodriguez-Crespo, Distance-dependent cellular palmitoylation of de-novo-designed sequences and their translocation to plasma membrane subdomains, J. Cell Sci. 115 (2002) 3119–3130.
[33] A.E. El-Husseini, D.S. Bredt, Protein palmitoylation: a regulator of neuronal development and function, Nat. Rev., Neurosci. 3 (2002) 791–802.
[34] T. Hayashi, G. Rumbaugh, R.L. Huganir, Differential regulation of AMPA receptor subunit trafficking by palmitoylation of two distinct sites, Neuron 47 (2005) 709–723.
[35] M. Veit, T.H. Söllner, J.E. Rothman, Multiple palmitoylation of synaptotagmin and the t-SNARE SNAP-25, FEBS Lett. 385 (1996) 119–123.
[36] X. Yang, C. Claas, S.K. Kraeft, L.B. Chen, Z. Wang, J.A. Kreidberg, M.E. Hemler, Palmitoylation of tetraspanin proteins: modulation of CD151 lateral interactions, subcellular distribution, and integrin-dependent cell morphology, Mol. Biol. Cell 13 (2002) 767–781.
[37] Y. Webb, L. Hermida-Matsumoto, M.D. Resh, Inhibition of protein palmitoylation, raft localization, and T cell signaling by 2-bromopalmitate and polyunsaturated fatty acids, J. Biol. Chem. 275 (2000) 261–270.
[38] S. DeSouza, J. Fu, B.A. States, E.B. Ziff, Differential palmitoylation directs the AMPA receptor-binding protein ABP to spines or to intracellular clusters, J. Neurosci. 22 (2002) 3493–3503.
[39] K. Takimoto, E.K. Yang, L. Conforti, Palmitoylation of KChIP splicing variants is required for efficient cell surface expression of Kv4.3 channels, J. Biol. Chem. 277 (2002) 26904–26911.
[40] D.M. Chetkovich, R.C. Bunn, S.H. Kuo, Y. Kawasaki, M. Kohwi, D.S. Bredt, Postsynaptic targeting of alternative postsynaptic density-95 isoforms by distinct mechanisms, J. Neurosci. 22 (2002) 6415–6425.
[41] J. Greaves, L.H. Chamberlain, Palmitoylation-dependent protein sorting, J. Cell Biol. 176 (2007) 249–254.
[42] A.E. El-Husseini, S.E. Craven, S.C. Brock, D.S. Bredt, Polarized targeting of peripheral membrane proteins in neurons, J. Biol. Chem. 276 (2001) 44984–44992.